

## Integer Quantum Hall Effect in Trilayer Graphene

A. Kumar,<sup>1</sup> W. Escoffier,<sup>1</sup> J. M. Poumirol,<sup>1</sup> C. Faugeras,<sup>1</sup> D. P. Arovas,<sup>2</sup> M. M. Fogler,<sup>2</sup> F. Guinea,<sup>3</sup>  
S. Roche,<sup>4,5</sup> M. Goiran,<sup>1</sup> and B. Raquet<sup>1</sup>

<sup>1</sup>LNCMI, CNRS-UPR 3228, INSA, UJF, UPS, 143 Avenue de Rangueil, 31400 Toulouse,  
France and 25 rue des Martyrs, 38042 Grenoble, France

<sup>2</sup>Department of Physics, University of California at San Diego, 9500 Gilman Drive, La Jolla, California 92093, USA

<sup>3</sup>Instituto de Ciencia de Materiales de Madrid, CSIC, Cantoblanco E28049 Madrid, Spain

<sup>4</sup>CIN2 (ICN-CSIC) and Universitat Autònoma de Barcelona, Catalan Institute of Nanotechnology, Campus de la UAB, 08193  
Bellaterra (Barcelona), Spain

<sup>5</sup>ICREA, Institució Catalana de Recerca i Estudis Avançats, 08010 Barcelona, Spain

(Received 18 April 2011; published 16 September 2011)

By using high-magnetic fields (up to 60 T), we observe compelling evidence of the integer quantum Hall effect in trilayer graphene. The magnetotransport fingerprints are similar to those of the graphene monolayer, except for the absence of a plateau at a filling factor of  $\nu = 2$ . At a very low filling factor, the Hall resistance vanishes due to the presence of mixed electron and hole carriers induced by disorder. The measured Hall resistivity plateaus are well reproduced theoretically, using a self-consistent Hartree calculations of the Landau levels and assuming an *ABC* stacking order of the three layers.

DOI: 10.1103/PhysRevLett.107.126806

PACS numbers: 73.43.-f, 61.72.Bb, 71.55.Cn, 73.61.Wp

**Introduction.**—More than 30 years after its initial discovery in two dimensional electron gases (2DEG), the integer quantum Hall effect (IQHE) remains one of the most fascinating phenomena in condensed matter physics [1]. The recent discovery of graphene [2] boosted this research field by providing a new 2D system where Dirac-like electronic excitations with Berry's phase  $\pi$  leads to a new form of IQHE [3,4], with plateaus at  $\sigma_{xy} = (n + \frac{1}{2})ge^2/h$ , where  $g$  is the Landau level degeneracy due to spin and valley degrees of freedom. A third type of IQHE was then reported in bilayer graphene, where the  $2\pi$  Berry's phase of charge carriers results in a conventional quantization sequence, except that the last Hall plateau is missing [5]. As the dynamics of charged carriers change every time an extra graphene layer is added, it was theoretically anticipated that the Landau level (LL) spectrum of  $N$ -layer graphene systems would result in distinctive IQHE features arising from an  $N\pi$  Berry's phase. In trilayer graphene, the zero-energy LL is expected to be twelvefold degenerate so that the Hall resistance plateau sequence follows the same ladder as in graphene, but the plateau at  $\nu = \pm 2$  should be missing [see Fig. 1(a)]. So far, most of the studies dedicated to IQHE in trilayer graphene have been restricted to theoretical calculations [6–11] while experimental data are limited [12,13], since the knowledge of the exact number of layers and their relative stacking order are challenging to establish unambiguously.

In this Letter, using both high field magnetotransport measurements and Raman spectroscopy, a trilayer graphene sample is clearly identified and allows us to report on the typical features of the fourth type of IQHE in graphene-based materials. Self-consistent Hartree

calculations of Landau levels [based on the Slonczewski-Weiss-McClure (SWMC) tight-binding model [14–16]] are favorably compared to the experimental data, allowing an unambiguous determination of the stacking order between layers, which turns out to be given by the *ABC* stacking geometry.

**Experimental technique.**—Many graphene flakes were deposited onto a  $d = 280$  nm thick thermally grown silicon oxide on silicon substrate (used as a back gate) using micromechanical exfoliation of natural graphite. Standard electron beam lithography and oxygen plasma etching were used to contact electrically one particular trilayer flake in the Hall bar geometry (see Supplemental Material [17] for technical details). For this annealed device, the gate voltage required to reach the charge neutrality point (CNP) is  $V_{\text{CNP}} = -13.75$  V, indicating the presence of a  $n$ -type residual doping estimated to  $n_0 = 0.85 \times 10^{12} \text{ cm}^{-2}$ . The Raman scattering spectrum was measured at room temperature using a confocal micro Raman scattering setup using He-Ne laser excitation ( $\lambda = 632.8$  nm) with  $\sim 1$  mW optical power focused on a  $1 \mu\text{m}$  diameter spot. The 2D band feature (also called  $G'$  feature) of this sample is shown in Fig. 1(a) (inset) and appears in the form of a multicomponent feature characteristic of multilayer graphene [18], different from the one observed for a monolayer graphene processed in the same way [also shown in the inset of Fig. 1(a)]. The experimental IQHE of the sample under study is displayed in Fig. 1(b), together with bilayer and monolayer graphene fingerprints of other samples. These samples have an equivalent carrier density and similar mobility (see legend of Fig. 1 for details). For graphene trilayer, the sequence of the Hall resistance plateaus is described by  $R_{xy} = h/\nu e^2$  where  $\nu = 6, 10, 14, \dots$

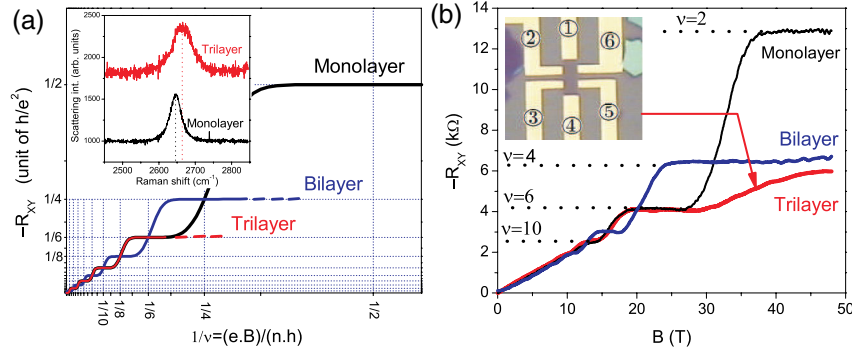


FIG. 1 (color online). (a) Schematic representations of the IQHE in mono-, bi-, and trilayer graphene. The degeneracy of the zeroth Landau level (LL) is fourfold degenerate in graphene, eightfold degenerate in bilayer graphene, and twelvefold degenerate in trilayer graphene, leading to a sequence of Hall resistance plateaus shifted by  $2h/e^2\Omega$ . Inset: Raman spectrum of trilayer graphene (red or top curve) and monolayer graphene (black or bottom curve) measured on the same substrate. (b) Experimental IQHE in tri-, bi-, and monolayer graphene for equivalent carrier density  $n = 3.4 \times 10^{12} \text{ cm}^{-2}$  and similar mobility  $\mu = 1200 \text{ cm}^2 \text{ V}^{-1} \cdot \text{s}^{-1}$ . The optical image of the trilayer graphene sample is shown in inset. As contact 1 was proven defective, a constant current of  $i = 1 \mu\text{A}$  is injected through contacts 2 and 4. The Hall resistance is measured between contacts 3 and 5.

Indeed, the IQHE in trilayer graphene is indistinguishable from its monolayer counterparts except at very high field where the  $\nu = 2$  quantized Hall resistance plateau is absent. We notice, however, that the Hall resistance slightly overshoots the  $\nu = 6$  resistance plateau at very high magnetic field. This surprising feature triggered the need for a detailed theoretical analysis of the LL spectrum [19,20] which goes beyond the simple considerations presented earlier in the introduction.

*Theoretical model.*—To model a gated graphene  $p$  layer, a self-consistent approach is used, integrating Gauss's law across the layers with  $p$  equations  $\phi_{j-1} - \phi_j = \frac{4\pi e d_j}{\kappa_j} \times \sum_{i=j}^p n_i$ , ( $j = 1, \dots, p$ ), with  $\phi_0 \equiv \phi_g$ , the gate potential. Here  $n_i$  is the total charge density (including positive ions) in layer  $i$  in units of  $-e$  ( $e > 0$ ), and  $d_j$  and  $\kappa_j$  are the separations and dielectric constants between layers  $j-1$  and  $j$  (cgs units). To this system we add the equation  $eV_g = \zeta - \zeta_g$ , where  $\zeta$  and  $\zeta_g$  are the electrochemical potentials for the multilayer and gate, respectively. We can set  $\mu_g = 0$  in the gate, so  $\zeta_g = -e\phi_0$ , whence  $eV_g = \zeta + e\phi_0$ . We may also set  $\phi_p \equiv 0$ . We take  $d_{j>1} = 3.4 \text{ \AA}$  between graphene layers and  $d_1 = 280 \text{ nm}$ , the gate separation in our device.

In a uniform magnetic field, we write  $n_j = N_j/2\pi\ell^2$ , where  $\ell = \sqrt{\hbar c/eB}$  is the magnetic length, and

$$N_j = \sum_a \left[ (u_{ja}^2 + v_{ja}^2)(f_{a\uparrow} + f_{a\downarrow}) - \frac{1}{p} \right], \quad (1)$$

where  $\{u_{ja}, v_{ja}\}$  are the normalized wave function amplitudes for the  $u$  and  $v$  sublattice sites on layer  $j$  in eigenstate  $a$ , and  $f_\sigma = f(E_a + \sigma\omega_Z)$  is the Fermi function for electrons of spin polarization  $\sigma$ , with  $\omega_Z \equiv \frac{1}{2}g\mu_B B$  and  $\mu_B$  the Bohr magneton. The  $-1/p$  term accounts for the ionic charge. We assume  $g = 2$  and do not account for any

exchange enhancement of the  $g$  factor. We have  $4\pi e^2 n_j = rBN_j$ , with  $r = 2e^2/B\ell^2 = 0.437 \text{ meV/T \AA}$ . The layer densities are then  $n_j = BN_j \times 2.419 \times 10^{10} \text{ cm}^{-2}/\text{T}$ .

If graphene contains charged impurities, the individual layer charge densities can be modeled as  $\tilde{n}_j = n_j + \Delta n_j$ , where  $\Delta n_j$  is the impurity charge density in units of  $-e$ . These stray charge densities are not known *a priori*, but given the observed experimental offset voltage  $\Delta V_g$ , an effective gate bias can be set as  $V_g + \Delta V_g$ . Assuming that the sample can be described by a single capacitor plate located at a distance  $d_s$  away from the gate, then the corresponding stray charge density writes  $\Delta n = \kappa_1 \Delta V_g / 4\pi e d_1$ . In a multilayer sample, the distribution of stray charge densities  $\Delta n_j$  is unclear, but we find that our results are quite insensitive to their specific rearrangement in between layers, although the best results are obtained for stray charges located on the top layer.

By defining  $U_j \equiv -e\phi_j$ , the final form of our self-consistent equations for the trilayer is then

$$\zeta - U_1 + rBx_s(\tilde{N}_1 + \tilde{N}_2 + \tilde{N}_3) = eV_g, \quad (2)$$

$$U_1 - U_2 + rBx(\tilde{N}_2 + \tilde{N}_3) = 0, \quad (3)$$

$$U_2 + rBx\tilde{N}_3 = 0, \quad (4)$$

where  $\tilde{N}_j = N_j + \Delta N_j$ , with  $\Delta N_j = 2\pi\ell^2 \Delta n_j$ ,  $U_0 = \zeta - eV_g$ , and  $U_3 \equiv 0$ . We have further defined  $x \equiv d/\kappa$  and  $x_s \equiv d_1/\kappa_1$ . The three unknowns are  $\zeta$ ,  $U_1$ , and  $U_2$ . To solve these equations self-consistently (to an accuracy of  $10^{-6}$ ), we use a modified Powell method subroutine, HYBRD1, from the MINPACK library.

To model the effects of disorder, we replace the density of states  $D(E) = \sum_a \delta(E - E_a)$  with  $\bar{D}(E) = \frac{1}{2W_0} \sum_a \Theta(W_0 - |E - E_a|)$ , where  $\Theta(x)$  is the Heaviside function. We then replace the Fermi function  $f(E)$  with

$$\bar{f}(E) = \frac{1}{2W_0} \int_{-W_0}^{W_0} dW \frac{1}{e^{(E+W-\xi)/k_B T} + 1} \quad (5)$$

$$= 1 - \frac{k_B T}{2W_0} \ln \left( \frac{1 + e^{(E+W_0-\xi)/k_B T}}{1 + e^{(E-W_0-\xi)/k_B T}} \right). \quad (6)$$

Here  $W_0$  is the half-width of a square distribution.

The energy eigenvalues  $E_a$  are obtained from diagonalization of the appropriate Hamiltonian for the trilayer. We employ an SWMC tight-binding parametrization of the local hopping amplitudes [14,15]. There are two possible stacking orders to consider: Bernal (*ABA*) and rhombohedral (*ABC*), each illustrated in Fig. 2. For the Bernal case, we take  $\gamma_0 = 3000$  meV,  $\gamma_1 = 400$  meV,  $\gamma_2 = -20$  meV,  $\gamma_3 = 300$  meV,  $\gamma_4 = 150$  meV, and  $\gamma_5 = 38$  meV. In addition, there is an on-site energy shift of  $\frac{1}{2}\Delta = 18$  meV for each *c*-axis neighbor, as well as the self-consistent local potential on each layer. For the rhombohedral case [16,21], the parameter  $\gamma_5$  does not enter. At wave vector  $\vec{k}$ , the in-plane component of the hopping leads to a

Wallace factor of  $S(\vec{k}) = e^{i\vec{k}\cdot\vec{\delta}_1} + e^{i\vec{k}\cdot\vec{\delta}_2} + e^{i\vec{k}\cdot\vec{\delta}_3}$ , or of  $S^*$ , where  $\vec{\delta}_{1,2,3}$  are the three nearest-neighbor separations. Expanding about the two inequivalent zone corners, one finds  $S(\vec{K} + \vec{q}) = -\frac{\sqrt{3}}{2}(q_x + iq_y)a_0$  and  $S(\vec{K}' + \vec{q}) = S^*(\vec{K} - \vec{q}) = \frac{\sqrt{3}}{2}(q_x - iq_y)a_0$ , where  $a_0 = 2.46$  Å. In the presence of a magnetic field, we have  $\vec{q} \rightarrow \vec{q} + \frac{e}{\hbar c}\vec{A} \equiv \frac{1}{\hbar}\vec{\pi}$ , where  $[\pi_x, \pi_y] = -i\hbar^2/\ell^2$ , assuming  $\vec{B}$  is along  $\hat{z}$ . We then define cyclotron ladder operators  $b$  and  $b^\dagger$  according to  $b = \mp(\pi_x - i\pi_y)\ell/\sqrt{2}\hbar$  at  $\vec{K}$  ( $-$ ) and  $\vec{K}'$  ( $+$ ). This results in  $S \rightarrow \xi b^\dagger$  near  $\vec{K}$  and  $S \rightarrow \xi b$  near  $\vec{K}'$ , where  $\xi = \sqrt{B/B_0}$  and  $B_0 = \phi_0/3\pi a_0^2 = 7275$  T, where  $\phi_0 = hc/e$  is the flux quantum. The Hamiltonian is written as an infinite rank matrix in Landau level index space. The results are obtained using a cutoff of the Landau level index of 300 (see [17]). The theoretical results for  $R_{xy}$  were obtained by assuming that there is a unique critical energy at the center of each disorder-broadened Landau level where extended states exist. The Hall conductivity changes by  $\Delta\sigma_{xy} = e^2/h$  as the electrochemical potential sweeps through these energies. When Zeeman splitting is neglected,  $\Delta\sigma_{xy} = 2e^2/h$ .

*Results.*—Figure 2 shows the LL energies and theoretical Hall resistance for both *ABC* and *ABA* stacking for gate voltage  $V_g = +50$  V, along with the experimental results for  $R_{xy}$  (the full set of IQHE data is reported in the Supplemental Material [17]). For fields up to 40 T, the measurements agree fairly well with the theoretical predictions for the *ABC* trilayer, and fail to reproduce the theoretical Hall plateau sequence for the *ABA* trilayer. The different plateau sequences for *ABC* and *ABA* trilayers arise due to the significant differences in their respective Landau level structures, as seen in Fig. 2. Indeed, the rhombohedral stacking order accounts for the absence of Hall plateaus at some filling factors, like  $\nu = 4, 8, 12, \dots$ , due to valley degeneracy arising from the inversion symmetry of the honeycomb lattice. In the absence of bias voltage, the *ABC* trilayer is inversion symmetric but lacks mirror symmetry as compared to the *ABA* trilayer [22]. The presence of an electric field across the graphene layers, due to the gate voltage induced charge redistributions [10,23], breaks the lattice inversion symmetry. Neglecting Zeeman splitting, quantum Hall steps of amplitude  $\Delta\sigma_{xy} = 2e^2/h$  should be observed for each plateau-to-plateau transition. This holds, in particular, for the Bernal type of stacking as the LLs originating from valleys  $K$  and  $K'$  are quite distinct from each other due to the absence of inversion symmetry. On the other hand, the *ABC*-stacked LL band structure is much less affected by electrostatic effects. At high enough magnetic field, the LLs evolve roughly by bunches of four and, when disorder effects are taken into account, lead to quantum Hall steps of  $\Delta\sigma_{xy} = 4e^2/h$ , as experimentally observed. Intriguingly, the IQHE fails to be reproduced at very low filling factor (high magnetic field and low carrier

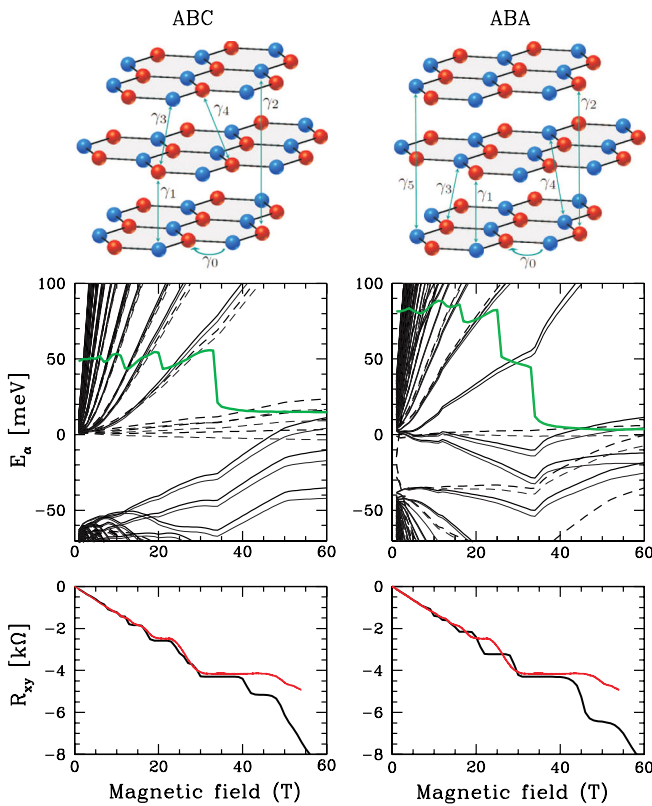


FIG. 2 (color online). Ball-and-stick model for a *ABA* and *ABC*-stacked trilayer graphene (top panel), theoretical Landau level structure (middle panel) and quantized Hall resistance (bottom panel) using:  $V_g = 50$  V,  $V_{\text{CNP}} = -13.75$  V,  $T = 4.2$  K,  $W_0 = 10$  meV and  $g = 2$ . In the middle panel, the solid and dashed curves indicate the Landau levels originating from valleys  $K$  and  $K'$ , respectively. Bottom panel: experimental (red line) and theoretical (black line) Hall resistance.

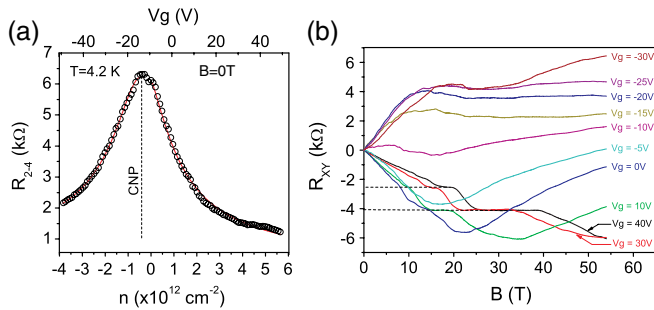


FIG. 3 (color online). (a) Longitudinal resistance as a function of carrier concentration at 4.2 K. (b) Hall resistance for various back-gate voltage in the vicinity of the CNP. Notice that the Hall resistance tends to vanish at  $V_g \approx V_{\text{CNP}}$  and very high magnetic field. For  $V_g \gg V_{\text{CNP}}$ , the expected quantum Hall effect in the graphene trilayer is recovered.

density). To further investigate this issue, we analyze the Hall resistance for various charge carrier concentrations close to CNP. Focusing at Fig. 3(b), we begin the analysis with the Hall resistance for  $V_g = +40$  V ( $n = 4.3 \times 10^{12} \text{ cm}^{-2}$ ), which displays well-defined quantized Hall plateaus. As the gate voltage is decreased, the Hall resistance plateaus are shifted at lower magnetic field as expected theoretically. On the other hand, as the Fermi energy is driven closer to CNP, the low field Hall effect is no longer linear reflecting the presence of electrons and holes that both contribute to transport. For  $V_g < +20$  V, the initial ratio between electron-hole density evolves as the magnetic field is increased to accommodate the field-induced redistribution of quantum states available in the lowest LL [24]. Actually, the electron and hole densities tend to equilibrate and consequently the Hall resistance vanishes at high field. This effect is a hallmark of the disordered 2DEG [25], where the presence of electron and hole puddles allows both types of carriers for a given Fermi energy close to CNP. The theoretical model presented earlier does not take into account such effects and therefore is not appropriate to describe the low-filling factor regime ( $\nu < 6$ ).

**Conclusion.**—A new form of IQHE in a gated trilayer graphene has been observed. The filling factor sequence associated with the quantized Hall resistance plateaus is identical to that for graphene, but the plateau at  $\nu = 2$  is missing. The experimental data are supported by a theoretical analysis which suggests that the measured trilayer sample has a rhombohedral stacking. The comparison with samples with higher mobility, e.g., in suspended or boron nitride-deposited graphene trilayers, will be very interesting [12].

This work is supported by EuroMagNET II program under EU Contract No. 228043, by the French ANR under Contract No. ANR-08-JCJC-0034-01, and by the technological platform of LAAS-CNRS (RTB network). D. P. A.

is supported by NSF Grant No. DMR-1007028. F. G. is supported by MICINN (Spain), Grants No. FIS2008-00124 and CONSOLIDER CSD2007-00010. M. Potemski is acknowledged for fruitful discussions.

- [1] K. v. Klitzing, G. Dorda, and M. Pepper, *Phys. Rev. Lett.* **45**, 494 (1980).
- [2] K. S. Novoselov, D. Jiang, F. Schedin, T. J. Booth, V. V. Khotkevich, S. V. Morozov, and A. K. Geim, *Proc. Natl. Acad. Sci. U.S.A.* **102**, 10 451 (2005).
- [3] K. Novoselov, A. Geim, S. Morozov, D. Jiang, M. Katsnelson, I. Grigorieva, S. Dubonos, and A. Firsov, *Nature (London)* **438**, 197 (2005).
- [4] Y. Zhang, Y. Tan, H. Stormer, and P. Kim, *Nature (London)* **438**, 201 (2005).
- [5] K. Novoselov, E. McCann, S. Morosov, V. Fal'ko, M. Katsnelson, U. Zeitler, D. Jiang, F. Schedin, and A. Geim, *Nature Phys.* **2**, 177 (2006).
- [6] H. Min and A. H. MacDonald, *Phys. Rev. B* **77**, 155416 (2008).
- [7] M. Ezawa, *J. Phys. Soc. Jpn.* **76**, 094701 (2007).
- [8] M. Nakamura and L. Hirasawa, *Phys. Rev. B* **77**, 045429 (2008).
- [9] M. Nakamura, L. Hirasawa, and K. I. Imura, *Phys. Rev. B* **78**, 033403 (2008).
- [10] M. Aoki and H. Amawashi, *Solid State Commun.* **142**, 123 (2007).
- [11] F. Zhang, J. Jung, G. A. Fiete, Q. Niu, and A. H. MacDonald, *Phys. Rev. Lett.* **106**, 156801 (2011).
- [12] T. Taychatanapat, K. Watanabe, T. Taniguchi, and P. Jarillo-Herrero, *Nature Phys.* **7**, 621 (2011).
- [13] L. Zhang, Y. Zhang, J. Camacho, M. Khodas, and I. A. Zaliznyak, *arXiv:1103.6023v1*.
- [14] J. C. Slonczewski and P. R. Weiss, *Phys. Rev.* **109**, 272 (1958).
- [15] J. W. McClure, *Phys. Rev.* **108**, 612 (1957).
- [16] J. W. McClure, *Carbon* **7**, 425 (1969).
- [17] See Supplemental Material at <http://link.aps.org/supplemental/10.1103/PhysRevLett.107.126806> for technical details and additional experimental results.
- [18] D. Graf, F. Molitor, K. Ensslin, C. Stampfer, A. Jungen, C. Hierold, and L. Wirtz, *Solid State Commun.* **143**, 44 (2007).
- [19] F. Guinea, A. H. Castro Neto, and N. M. R. Peres, *Phys. Rev. B* **73**, 245426 (2006).
- [20] D. P. Arovas and F. Guinea, *Phys. Rev. B* **78**, 245416 (2008).
- [21] F. Zhang, B. Sahu, H. Min, and A. H. MacDonald, *Phys. Rev. B* **82**, 035409 (2010).
- [22] M. Koshino and E. McCann, *Phys. Rev. B* **81**, 115315 (2010).
- [23] M. Koshino, *Phys. Rev. B* **81**, 125304 (2010).
- [24] J.-M. Pouchard, W. Escoffier, A. Kumar, B. Raquet, and M. Goiran, *Phys. Rev. B* **82**, 121401 (2010).
- [25] G. M. Gusev, E. B. Olshanetsky, Z. D. Kvon, N. N. Mikhailov, S. A. Dvoretzky, and J. C. Portal, *Phys. Rev. Lett.* **104**, 166401 (2010).